



Increased Ion Throughput Using Tristate Ion-Gate Multiplexing

Journal:	<i>Analyst</i>
Manuscript ID	AN-ART-08-2019-001585.R1
Article Type:	Paper
Date Submitted by the Author:	27-Sep-2019
Complete List of Authors:	Kwantwi-Barima, Pearl; Washington State University, Department of Chemistry Reinecke, Tobias; Washington State University, Department of Chemistry Clowers, Brian; Washington State University, Department of Chemistry

Increased Ion Throughput Using Tristate Ion-Gate Multiplexing

Pearl Kwantwi-Barima, Tobias Reinecke, Brian H. Clowers*

Department of Chemistry, Washington State University, Pullman, WA 99164

*Corresponding Author: brian.clowers@wsu.edu

ABSTRACT

For time dispersive ion mobility experiments detail control over the mechanism of ion beam modulation is necessary to establish optimum performance as this parameter greatly influences the temporal width of the ion beam arriving at the detector. When sampling continuous ion sources the temporal sampling or the incoming ion beam is often achieved by the electronic modulation of a grid or electric field. Not surprisingly, the rate at which a given ion population traverses this gating region is directly proportional to an ion's population and the applied electric field. This scenario establishes conditions where discrimination of the incoming ion beam may occur when the ion gate modulation rate is minimized. Recent developments in the mechanical construction of ion gates and their subsequent operation suggest that the mobility discrimination during ion gating may be minimized, however, it remains unclear how this behavior will translate to ion beam multiplexing approaches. In this present work, we compare the performance levels of the tri-state ion shutter (3S-IS) to the two-state ion shutter (2S-IS) using a series of Fourier transform ion mobility mass spectrometry (FT-IMMS) experiments. The performance of the two different shutter operating principles were evaluated using ion multiplexing using tetraalkylammonium salts (TXA ions; T5-T8, T10,T12) bradykinin, and a set of reversed sequence isomeric pentapeptides using a variety of different ion gate frequency sweeps. Noticeable increases in ion throughput were observed for the 3S-IS with 95 % and 45 % increases in ion counts for the T5 and T12 ions respectively compared to the 2S-IS. Similarly, a 27 % and 55 % increase in ion counts was observed for the $[M+2H]^{2+}$ and $[M+H]^+$ ions of bradykinin, respectively. In addition, a 10 % increase in resolving power was also observed for the 3S-IS compared to the 2S-IS. Overall, utilization of the 3S-IS effectively minimizes both discrimination of slower ions and the impact of gate depletion effect common to traditional ion gating techniques.

1
2
3
4
5 **Keywords:** Ion Mobility Spectrometry; Mass Spectrometry; Multiplexing; Ion
6 Discrimination; Ion Gating
7
8
9
10
11
12
13
14
15
16
17
18
19
20
21
22
23
24
25
26
27
28
29
30
31
32
33
34
35
36
37
38
39
40
41
42
43
44
45
46
47
48
49
50
51
52
53
54
55
56
57
58
59
60

INTRODUCTION

With the introduction of commercial ion mobility-mass spectrometry (IM-MS) platforms and the drive to explore biological systems using the mobility as an additional dimension of information,¹⁻² the application space of ion mobility spectrometry (IMS) has expanded well beyond its established role for detecting explosives,³ illicit narcotics,⁴ and chemical warfare agents (CWAs).⁵⁻⁶ Specifically, IM-MS finds a growing role as a multidimensional separation tool for analysis of mixtures such as peptides,⁷ protein complexes,⁸⁻⁹ protein fragments,¹⁰ or probing the effects of drug protein-interactions.¹¹ Despite the increasing availability and broad applicability, IMS is a comparably low resolution separation method and efforts of enhancing its separation factors and selectivity are of considerable benefit.

In a traditional signal averaged drift tube IMS experiment, a small packet of ions is injected into the drift tube where the ions separate based on the differences in mobility in a neutral drift gas under the influence of a weak electric field. Because the period between ion gating cycles is limited to the slowest moving ion population, the single gate, signal averaged (SGSA) drift tube experiment suffers from extremely low duty cycles of less than 1 % with more than ~ 99 % of the gas-phase ion population discharging on the closed ion gate. Furthermore, in order to maximize separation between different ion populations, reducing the initial width of the ion packet is paramount as this parameter is inversely proportional to resolving power.¹²

This latter point is particularly relevant for modern IM-MS instrumentation where high levels of resolution and speed are needed for both separation domains. For broadband, high-resolution ion mobility measurements using the SGSA technique, narrowing the arrival time distribution in the mobility domain logically yields narrower ion distributions at the detector which places increased demands on the mass analyzer with respect to increased sampling rates. Stated differently, for time-dispersive, high resolution IMS measurements, many mass analyzers are not suitable as detectors because a sampling rate of ~2-3 orders of magnitude greater than the SGSA experiments is required in order to accurately capture the arrival time distribution of ions. To address this sampling rate deficiency, early efforts to couple IMS to slow detectors required the use of a

1
2
3 second gate (scanning gate) at the end of the drift region.^{13,14} In these experiments, the
4 time delay between the opening event of the first and second gate was varied making it
5 possible to sample the mobility spectrum in discrete slices. However, this method
6 further reduces ion utilization efficiency and drastically extends acquisition times.
7
8
9

10
11 Regardless of the ion detector used, ion multiplexing techniques based upon Hadamard
12 and Fourier-based ion gate modulation techniques aim to alleviate the poor duty cycle
13 experienced with signal averaged drift tube IMS.¹⁵ Because both techniques modulate
14 the signal outside of the time domain, both are generally compatible with a range of
15 detector speeds. However, the ease of implementing the Fourier transform IMS
16 experiment (i.e. only the start and stop times of the mass and mobility domains need be
17 synchronized) has proven particularly useful when coupling IMS separations to ion trap
18 mass analyzers,¹⁶ including Orbitraps,¹⁷ and Fourier transform ion cyclotron resonance
19 (FT-ICR) systems.¹⁸ Compared to the dual-gate Hadamard experiment where the ion
20 gate pulsing cycles must be synchronized with the scanning events in the m/z domain,
21 in a dual gate FT-IMS experiment both gates are opened and closed simultaneously,
22 while the frequency of the opening and closing events is linearly swept. This procedure
23 enhances the theoretical duty cycle to 25 %, however, the attainable resolving power
24 critically depends on the frequency range of the sweep.¹⁶ While the drive to couple high
25 resolution drift-tube IMS measurements with high resolution mass analyzers is
26 understandable, there is, unfortunately, a significant deleterious impact of high ion
27 gating frequencies on the transmission of low mobility ion species. The inability of slow
28 moving ions to traverse the region of influence surrounding the ion gate during opening
29 and closing event establishes a bias against slow moving ions that can succinctly be
30 categorized as ion gate depletion. This effect is well documented for Bradbury-Nielsen
31 (BN) ion shutters and has been noted by numerous research groups.^{19,20,21}
32
33
34
35
36
37
38
39
40
41
42
43
44
45
46
47

48 Regardless of the ion injection method used for drift-cell IMS systems, concerns over
49 mobility bias exist. The Tyndall and Bradbury-Nielsen (BN) shutter are perhaps the
50 most commonly used ion gate shutter designs for high-pressure IMS systems while
51 more complex ion funnel trapping systems are widely used in lower pressure drift cell
52 applications.²² Despite range of pressure and different ion injection mechanism, mobility
53
54
55
56
57
58
59
60

1
2
3 bias still remains. In an effort to minimize ion discrimination for lower mobility ions,
4 Ibrahim et al,²³ altered the ion trapping conditions within an ion funnel by using helium at
5 a slightly lower pressure than the a drift cell filled with nitrogen. The experimental
6 conditions established in the ion funnel using helium during ion ejection demonstrated
7 improved levels of sensitivity for lower mobility ions by an order of magnitude in
8 comparison to when nitrogen is used in the ion funnel trap. While the conditions used by
9 Ibrahim et al, ²³ illustrate a new method for lower-pressure drift cell systems, this
10 method does not translate to drift cells much above 10 torr.
11
12
13
14
15
16
17

18 Recently, a tri-grid ion shutter configuration was introduced by Langejuergen et al.²⁴
19 which presents a fully functional form of the original concepts proposed by Blanchard et
20 al. related to ion-wells.²⁵ While the tri-grid ion shutter greatly eases the speed,
21 assembly, and levels of robustness compared to the BN shutter, the first FT-based
22 multiplexing results illustrated that this type of ion shutter also suffered from gate
23 depletion at high frequencies.²⁶ However, recent improvements to the operation of the
24 tri-grid shutter by Kirk et al.²⁷ in the form a tri-state, tri-grid (3S-IS) ion shutter
25 demonstrate significantly less ion depletion in the SGSA mode of operation. In fact, the
26 experiments by Kirk et al. reported minimal levels of ion gate depletion for ion gate
27 pulse widths as low as 1 μ s.^{27,28} Building upon the efforts of Kirk et al. using an
28 independent implementation of the concept, the aim of the present work is to investigate
29 the utilization of the 3S-IS shutter for ion multiplexing with Fourier transform IMS using a
30 Faraday plate as a detector and also a linear ion trap. The comparison between the 3S-
31 IS and the two-state configuration using a series of tetraalkylammonium salts (T5-T8,
32 T10, T12 ions) and peptides (bradykinin and a set of reversed sequence
33 pentapeptides), we show significant improvement in both resolving power and ion
34 current delivered to the detector.
35
36
37
38
39
40
41
42
43
44
45
46
47
48
49

50 **EXPERIMENTAL**

51 *Chemicals and Reagents.* The target analytes were chosen as compounds with different
52 functional groups and range of reduced mobilities. These included tetraalkylammonium
53 salts (TXA (T5-T8, T10, T12)), bradykinin, and a set of reversed sequence
54
55
56
57
58
59
60

1
2
3 pentapeptides all sourced from Sigma Aldrich. These analytes were used to compare
4 the tristate ion shutter (3S-IS) to the two-state ion shutter (2S-IS). In addition to the
5 analytes listed above, HPLC grade methanol and 0.1% formic acid (ACS reagent grade,
6 $\geq 97\%$ or 98% purity) were purchased from Sigma Aldrich Chemical Co. (Milwaukee,
7 WI, USA) The TXA ions were formulated at a concentration of $50\ \mu\text{M}$ in HPLC grade
8 methanol, whereas, bradykinin and the reversed sequence pentapeptide mixture were
9 diluted to concentrations of $20\ \mu\text{M}$ and $50\ \mu\text{M}$ in HPLC grade methanol with 0.1% formic
10 acid, respectively.
11
12
13
14
15
16
17

18
19 *Atmospheric Pressure Evaluation of the Tri-State Ion Shutter.* Initial evaluation of the
20 3S-IS was performed using a standalone, atmospheric pressure, dual shutter ion
21 mobility spectrometer modeled after the design reported by Reinecke and Clowers.²⁹
22 The aforementioned PCB-IMS comprised of a 10.02 cm desolvation region and a drift
23 tube length of 11.40 cm (with a length of 10.40 cm between the first and second gates).
24 We note that in order to obtain signal averaged ion mobility spectra, the second gate of
25 the PCB-IMS was set to open state throughout the experiment and a Faraday plate was
26 used for detection. The amplifier used for the standalone ion mobility measurements
27 was a Keithley 427 amplifier (current to voltage) which amplifies the current produced
28 by the ions discharged on the Faraday plate with a rise time of $30\ \mu\text{s}$ and an
29 amplification of $10^9\ \text{V/A}$.
30
31
32
33
34
35
36
37
38

39 *Multiplexed, Atmospheric Pressure, Dual-Shutter Ion Mobility-Mass Spectrometer.* The
40 mass-selected mobility spectra for the target analytes were obtained using the same
41 PCB-IMS mentioned above coupled to a linear ion trap mass spectrometer, LTQ-XL
42 (Thermo Fisher Scientific, Thousand Oaks, CA) by frequency encoding the mobility
43 data. With the linear ion trap mass spectrometer as the detector, the ion trap was filled
44 for fixed period of time by setting the target accumulation population to an improbably
45 large values as AGC could not be turned off in the standard LTQ-XL control software.
46 Using this scheme a maximum injection time of 100 ms and m/z ranges of 50-500, 250-
47 700, 500-1070 were used for the for the analysis of the reversed sequence
48 pentapeptide, TXA salts, and bradykinin, respectively. The synchronized gating
49
50
51
52
53
54
55
56
57
58
59
60

1
2
3 frequency for the frequency modulated IMS experiments was swept from 5 - 10,005 Hz,
4 5 - 15,005 Hz and 5 - 20,005 Hz over the course of 8 minutes. The following operating
5 conditions were also used for the standalone ion mobility measurements. The analytes
6 were electrosprayed at a flow rate of 3 $\mu\text{L}/\text{min}$ through a 75 μm glass capillary. An
7 electro spray ionization voltage of 3000 V was used relative to the potential of the first
8 IMS electrode held at 12000 V. These conditions established an electric field gradient
9 of ~ 467 V/cm through the drift region. The IMS was operated under atmospheric
10 pressure (~ 690 Torr in Pullman WA) and maintained at room temperature (23 $^{\circ}\text{C}$). A
11 clean nitrogen gas flow of 2 L/min was allowed into the rear of the drift tube. The ions
12 were gated using a two-state (three-grid ion shutter) and tri-state ion shutter (three-grid
13 ion shutter with two closed states) following the first reports by Langejuren et al. and
14 Kirk et al., respectively.^{24,30} The first and second ion shutters were operated using a set
15 of open-source ion gate pulsers triggered using a National Instruments Multifunctional
16 DAQ (USB-6351, National Instruments, Austin, TX) that supplied the user-defined
17 waveforms needed for the multiplexing experiments.³¹ For both the standalone and IM-
18 MS experiments, the waveforms were streamed to the ion gate pulsers using the
19 NIDAQ Tools module extensions for IGOR Pro (Lake Oswego, OR).
20
21
22
23
24
25
26
27
28
29
30
31
32
33

34 *Tri-Grid Ion Shutter Configuration.* As mentioned previously, a detailed description of
35 the two-state three-grid ion shutter (2S-IS) can be found in a recent publication by
36 Langejuren et al.²⁴ and Reinecke and Clowers.²⁹ Structurally, the gating
37 arrangement follows that of the report by Reinecke and Clowers with each 100 μm wide
38 grid being separated from the adjacent grid by a 250 μm Teflon spacer.²⁹ This brings
39 the total mechanical width of the gating apparatus to approximately 850 μm , however,
40 the complexity of the fields and the region to which ions are confined spans
41 approximately 250 μm . To open the ion gate the center grid is connected to a resistor
42 voltage divider that provides the necessary voltage drop that allows the ions to pass
43 through the gate. In order to close the gate, a higher potential is applied to the center
44 grid, reversing the field in the region between first and center grid and thus stopping the
45 ions at the end of the desolvation region. To completely close the gate, a potential of
46 120 V was applied in order to stop ions from entering the drift region.
47
48
49
50
51
52
53
54
55
56
57
58
59
60

1
2
3
4
5 Given the focus of the manuscript, the core operation principles of the 3S-IS are worth
6 describing and are shown in Figure 1. In this diagram, source 1 (S1) and source 2 (S2)
7 are ion gate pulsers connected in series, while S1 is set to output a negative voltage
8 when turned on and S2 a positive voltage, respectively. Analogous to the 2S-IS, to open
9 the ion shutter during an opening time t_{open} , both sources S1 and S2 are off (outputting
10 0 V) and thus Grid₂ is connected to the center potential between Grid₁ and Grid₃
11 creating a field that allows ions to pass through the ion gate and enter the drift region.
12 For the 3S-IS, the closed state (t_{close}) is comprised of two stages: the pushing stage
13 (t_{push}) followed by the wait time (t_{wait}). In the pushing stage, a positive voltage is applied
14 to Grid₂ (S1 is off, S2 is on) to push all remaining ions located between Grid₂ and Grid₃
15 into the drift tube while also reversing the field between Grid₁ and Grid₂ and thus
16 stopping all ions at Grid₁. Subsequently, during the wait time (t_{wait}), a negative potential
17 is applied to Grid₂ (S1 is on, S2 is off) allowing ions to advance from Grid₁ to Grid₂. This
18 combination of pushing stage and wait time is what effectively leads to the significantly
19 reduced gate depletion effect observed with the 3S-IS.²⁷
20
21
22
23
24
25
26
27
28
29
30

31 32 **RESULTS AND DISCUSSION**

33
34 Using a set of tetraalkylammonium salts (TXA), bradykinin, and a set of reversed
35 sequence pentapeptides, the goal of the present study is to investigate and compare
36 the performance levels of the 3S-IS to the 2S-IS in FT-IMS experiments using both
37 standalone and hybrid MS instrumental configuration. The motivations for these
38 experiments are directly aimed at maximizing the levels of ion current reaching the
39 mass analyzers for low mobility ions which has direct bearing on present and future
40 efforts to assess arrival time distributions for large gas-phase complexes.
41
42
43
44
45
46
47

48 As a first step both the 3S-IS and 2S-IS principles were verified using signal averaged
49 mode of operation using a standalone IMS system. Figure 2 depicts the signal averaged
50 ion mobility spectra of TXA salts (T5-T8, T10, T12) at 20 μs , 50 μs , and 100 μs gate
51 pulse width (GPW) for both shutter principles. Approximately 1000 spectra were
52 averaged in the SA mode. The black trace in each spectrum in Figure 2 represents
53
54
55
56
57
58
59
60

1
2
3 spectra generated using the 2S-IS. At 100 μ s GPW, the target analyte ions T5-T8, T10
4 and T12 were all clearly identified when both ion shutter principles were employed.
5
6 However, the amount of target analyte ions detected when using the 3S-IS was
7
8 significantly higher; there is an approximately 100 % increase in peak intensity for the
9
10 target analyte ions with higher reduced mobility (T5-T8) and about 150 % increase for
11
12 target analytes with lower reduced mobility (T10,T12). The higher intensity signals for
13
14 the slower ions illustrates a significant reduction in the ion gate depletion effect.
15
16 Subsequently, by reducing the GPW to 50 μ s, only the target analyte ions T5-T8 were
17
18 identified with the 2S-IS while using the 3S-IS all analyte ions including T10 and T12
19
20 were clearly visible. Further reducing the GPW to 20 μ s, resulted in no target analyte
21
22 ions being observed using the 2STGIS, whereas, all the target analyte ions (i.e. T5-T8,
23
24 T10, and T12) were observed using the 3S-IS. The representative spectra in Figure 2
25
26 re-emphasizes the results reported by Kirk et al. when the ion counts of the DMMP
27
28 dimer ions increased by 400 % when using the tristate ion shutter,^{27, 28}

29
30 While encouraging, additional investigation was required to realize the ultimate goal of
31
32 using the 3S-IS for multiplexing experiments. Specifically, various working parameters
33
34 of the 3S-IS were critically investigated in order to optimize the pulsing sequence for
35
36 multiplexed ion gate operation. In a traditional FT-IMS experiment, the ion gates are
37
38 each operated at a 50% duty cycle with the assumption that the duty cycle is highly
39
40 correlated to the amount of ions transferred into the MS. However, in order to achieve a
41
42 50% duty cycle using the 3S-IS, both the open stage (t_{open}) and the closed state (t_{close})
43
44 must be set to a 1:1 ratio. Consequently, the duration of the t_{push} equal to the duration of
45
46 the t_{wait} , i.e. t_{push} and t_{wait} both represent 25% of one gating period in order to achieve a
47
48 50 % duty cycle. Placing these working principles in context, the ratio of the respective
49
50 pushing, waiting, and closing times needs to be carefully adjusted when applying the ion
51
52 shutter concept to the multiplexing experiment as ion multiplexing experiments critically
53
54 rely upon the ability of the system to produce sequential ion gate releases with a high
55
56 degree of fidelity. Because ion gating events in a multiplexing are often located in close
57
58 temporal proximity, the following set of experiments aims to answer the simply question:
59
60

1
2
3 What is the minimum delay between subsequent ion gating events that minimize bias in
4 mobility?
5
6
7

8 To answer this question, the following experiment was performed to characterize the
9 gating behaviour of the 3S-IS, in particular to obtain an estimate for the maximum
10 frequency where the 3S-IS is still capable of providing clean gating events. Therefore,
11 two subsequent ion injections were investigated, while subsequently decreasing gate
12 pulse widths. This allows for a performance assessment of the experimental data with
13 respect to an ideal gating event which theoretically yields identical peak shapes and
14 intensities, for both peaks generated from the first and second ion injections. However,
15 as the data demonstrate, deviations from the ideal exist. Due to diffusion of the injected
16 ion packets it is not possible for the employed system to detect two distinct peaks
17 released from two comparatively short, adjacent ion gating events. Therefore, a single
18 pulse spectrum was recorded first and then subtracted from the double pulse spectrum
19 in order to obtain only the spectrum generated by the second pulse of the double pulse
20 sequence, allowing comparison to the intensity and shape of an ion peak resulting from
21 a single ion injection.
22
23
24
25
26
27
28
29
30
31
32
33

34 Figure 3A depicts the results of the double release experiment for a GPW of 100 μs
35 (t_{push} and t_{wait} were set to 50 μs). As seen from the top spectrum, two overlapping peaks
36 are observed for the double pulse sequence of the T5 ion suggesting similar intensity
37 and shape for the peak produced by the first and second ion injections. A similar result
38 is found for the T12 ion where the subtracted spectrum reveals that the second pulse
39 produces approximately the same ion intensity than the first one. However, when using
40 a 50 μs GPW (t_{push} and the t_{wait} were set to 25 μs), the subtracted spectrum produced a
41 result slightly higher in ion intensity than the single pulse spectrum for both T5 and T12
42 ion (i.e. the intensity of the peak produced by the second ion injection is higher than the
43 peak from the first ion injection). This result suggest that a 25 μs pushing period is
44 insufficient to fully eject all of the target analyte ions into the drift tube and thus some of
45 the analyte ions from the first ion injection are being trapped in the region between Grid₂
46 and Grid₃ and subsequently released at the second ion injection. This would result in a
47
48
49
50
51
52
53
54
55
56
57
58
59
60

1
2
3 slight increase in ion intensity for the second pulse. Further decreasing the GPW to 20
4 μs (t_{push} and $t_{\text{wait}} = 10 \mu\text{s}$) intensifies the described effect as can be seen in Figure 3A.
5
6 The subtracted spectrum is significantly higher in ion intensity (100 % more) than the
7
8 single pulse spectrum. Considering an ideal system, based on the velocity of the target
9
10 ions, a $t_{\text{push}} = 10 \mu\text{s}$ should be able to completely move all the target analyte ions into
11
12 the drift tube. However, there are two major factors that could contribute to this non-
13
14 ideality observed in the experiment done in Figure 3; the size of the grids is non-zero
15
16 (100 μm in width) and the electric field between the grids extends beyond the physical
17
18 structure of the ion gate (fringe fields) both leading to a longer distance the ions need to
19
20 travel in order not to be captured by the reversed field applied during the waiting period.
21

22 To put the results into the framework of the FT-IMS experiment, the results of the
23
24 double gating experiments are translated into their corresponding gating frequencies.
25
26 Recognizing that the gating period is defined as one complete waveform cycle and
27
28 using the experiments shown in Figure 3 as an example, a 20 μs GPW translates into a
29
30 period of 40 μs , which corresponds to a frequency of 25 kHz (frequency = 1 / period).
31
32 Analogously, a 50 μs GPW translates to a period of 100 μs , and thus a frequency of 10
33
34 kHz and a period of 200 μs corresponds to a frequency of 5 kHz. Therefore, based on
35
36 data presented in Figure 3, operating the gates up to a maximum frequency of 10 kHz
37
38 (100 μs GPW) in an FT-IMMS experiment should provide a reasonable compromise
39
40 between ideal gating behaviour and a functional amount of points across an ion peak
41
42 after fourier transforming the raw spectrum.

43 Building upon the stand-alone 3S-IS experiment, the IMS was coupled to an LTQ to
44
45 evaluate the lessons learned when performing the FT-IMMS. Figure 4 depicts the
46
47 frequency encoded mobility spectra obtained using the LTQ system for both the 3S-IS
48
49 and the 2S-IS at different frequency chirp ranges for TXA salts (T5-T8, T10, T12). The
50
51 frequency ranges applied to the gates were 5 - 10,005 Hz, 5 - 15,005 Hz and 5 -
52
53 20,005 Hz for a duration of 8 minutes. Both gates were operated at a 50 % duty cycle,
54
55 which corresponds to an overall duty cycle (ion utilization) of 25 %. Figure 4 illustrates
56
57 the increase in ion intensities for the target analyte ions using the 3S-IS compared to
58
59
60

1
2
3 the 2S-IS. At the gating frequency of 5-10,005 Hz, as reported in Table 1, the ion counts
4 recorded for T5 and T12 with the 3S-IS were 2.05×10^4 and 6.69×10^3 corresponding to
5 a 95.2 % and 49.7 % increase for T5 and T12 ions respectively in comparison to the 2S-
6 IS. Similarly, the resolving power for the 3S-IS increased by 19.7 % and 25.5 % for T5
7 and T12 ion respectively in comparison to the 2S-IS. Aside the differences observed
8 between the 3S-IS and the 2S-IS in terms of ion counts and resolving power,
9 differences at different gating frequencies for the individual shutter principles were
10 observed. Based on the conclusion made from the results obtained in Figure 3, it is
11 expected that the spectrum recorded at lower gating frequency (10 kHz) should have
12 better results in terms of ion counts and resolving power than those obtained at higher
13 frequency such as 15 kHz, 20 kHz. Therefore, from Figure 4, significant differences in
14 ion intensities are noted when comparing the spectra obtained at a gating frequency of
15 5 - 20,005 Hz to those acquired using 5 - 10,005 Hz, with the latter producing much
16 higher ion counts than the former. Reduced levels of total ion current are expected for
17 linear frequency sweeps that extend to higher frequencies as diffusion limits the
18 capacity of the system to resolve differences between closely spaced ion injection
19 pulses. Essentially, if two adjacent ion gate releases produce peaks that diffuse into
20 each other at higher frequencies, only a change in dc-current would be noted and not
21 additional mobility information. We note that the higher ending gating frequencies
22 (15,005 Hz and 20,005 Hz) depicted in Figure 4 illustrate the capability of the 3S-IS to
23 minimize the ion gate depletion effect while simultaneously yield higher resolving power
24 in comparison to the 2S-IS. While diffusion between adjacent ion gate releases place an
25 upper bound on the frequencies, and by extension the resolution achieved, using the
26 FT-IMS technique the 3S-IS does produce another benefit worth considering for hybrid
27 instrumentation that includes a mass analyzer--enhanced ion throughput. Figure 5
28 depicts two raw signals traces for the FT-IMMS experiment with each trace
29 corresponding to the 3S-IS and 2S-IS for the T5 ion. The 3S-IS trace shown in Figure 5
30 illustrates a continuous rise in the ion intensity over the course of the experiment for the
31 3S-IS while the average, mass-selected ion current for the 2S-IS remains largely
32 constant during the course of the experiment. The origins of this behavior are the
33 subject of continued investigation, however, the increase is attributed to a small trapping
34
35
36
37
38
39
40
41
42
43
44
45
46
47
48
49
50
51
52
53
54
55
56
57
58
59
60

1
2
3 well established within the tri-grid shutter operated in the 3S-IS mode. Most importantly,
4 this increase in ion current may be especially beneficial where deisotoping routines are
5 necessary to aid in spectral interpretation.
6
7

8
9
10 In order to evaluate the impact of the 3S-IS on analytes that differ from the TXA salts, a
11 comparison between the 3S-IS and 2S-IS was performed using bradykinin as it
12 produces both single and doubly charged species. The +1 charge state of bradykinin
13 ($[M+H]^+$) has a larger mass-to-charge ratio (m/z) of 1061 ($K_0 = 0.664 \text{ cm}^2/V\text{-}1\text{s}^{-1}$) than
14 the TXA T12 ion, which has a m/z of 691 ($K_0 = 0.701 \text{ cm}^2/V\text{-}1\text{s}^{-1}$). Figure 6 depicts the
15 results for mass-selected mobility spectra obtained from the FT-IMMS experiment for 20
16 μM bradykinin examined from 5-10,005 Hz over 8 minutes using both the 3S-IS and the
17 2S-IS. To illustrate the respective benefits of signal gains and resolving power, Figure
18 6A and 6C shows the unnormalized spectra and Figure 6B and 6D are the zoomed-in
19 spectra. The ion counts and the resolving power of the 3S-IS was higher than that of the
20 2S-IS for the bradykinin (+1,+2 charge states) analyte ion as observed in Table 1. At the
21 gating frequency used for the data acquisition shown in Figure 6, the ion counts
22 recorded for $[\text{bradykinin}+2\text{H}]^{2+}$ and $[\text{bradykinin}+\text{H}]^+$ were 6.25×10^4 and 1.35×10^3
23 respectively corresponding to a 27.8 % increase for $[\text{Bradykinin}+2\text{H}]^{2+}$ and 55.1 %
24 increase for $[\text{Bradykinin}+\text{H}]^+$ for the 3S-IS in comparison to the 2S-IS. Similarly, the
25 resolving power for the 3S-IS increased by 7.6 % and 16.1 % for $[\text{Bradykinin}+2\text{H}]^{2+}$ and
26 $[\text{Bradykinin}+\text{H}]^+$ respectively in comparison to the 2S-IS. Though modest gains, these
27 are significant in that only the operating principle of the shutter was changed and not the
28 physical dimensions. The data shown in Figure 6 also illustrate the relative benefits due
29 to a reduced ion gate depletion effect as the bradykinin +1 charge state has a longer
30 drift time than the +2 charge state. Therefore, from Figure 6, we observe lower ion
31 discrimination for the +1 charge state (less gate depletion effect) when using the 3S-IS
32 whereas a significant ion discrimination is observed with the 2S-IS.
33
34
35
36
37
38
39
40
41
42
43
44
45
46
47
48
49
50

51 In a concluding set of experiments the unique size-to-charge separation ability of IMS
52 which enables isomer separation was investigated and displayed in Figure 7 with
53 baseline separation of two isomeric reversed sequence pentapeptide mixture ($[\text{Ser-Asp-}$
54
55
56
57
58
59
60

1
2
3 Gly-Arg-Gly], [Gly-Arg-Gly-Asp-Ser]). Figure 7 displays the mass selected mobility
4 spectra for the singly charged ion species obtained through the FT-IMMS experiment
5 from 5-10,005 Hz for 8 minutes using the 3S-IS. The bottom spectrum depicts the singly
6 charged ion populations of the individual peptides and the top spectrum represents the
7 single charged ions of the peptide mixture. The separation of the singly charged ions
8 was due to the small differences in their conformational structure measurable as ion-
9 neutral collision cross section (CCS). The CCS values calculated from the experimental
10 measurements were 206 Å² for [SDGRG+H]⁺ and 212 Å² for [GRGDS+H]⁺. These CCS
11 values align well with reported literature values for the given compound ([SDGRG+H]⁺ ,
12 [GRGDS+H]⁺ at 204 Å² ³² and 212.7 Å² ³³ respectively). This translates to a difference
13 of approximately 3 % in CCS between the two singly charged species. While baseline
14 resolution of these two species was not achieved using the mixture, the clear
15 discrimination between the two isomers highlights the capacity of the multiplexing
16 systems combined with the 3S-IS to support analytical campaigns requiring isomeric
17 separation. For reference the resolving powers for the reversed sequence pentapeptide
18 mixture using the 3S-IS were 79 for SDGRG and 57 for GRGDS. While the resolving
19 powers for the individual species were 66 for SDGRG and 62 for GRGDS. It is worthy to
20 note that comparison spectra for the 2S-IS was not provided as this mode of operation
21 was unable to produce data with any meaningful degree of separation under the present
22 experimental conditions.
23
24
25
26
27
28
29
30
31
32
33
34
35
36
37
38

39 CONCLUSION

40
41 Through a robust comparison between the 3S-IS and 2S-IS principles, we clearly
42 demonstrate the capacity of the 3S-IS to increase the ion current delivered to an ion
43 detector while simultaneously enhancing the resolving power for drift-tube IMS
44 experiment equipped with a tri-grid ion shutter. Compared to previous efforts
45 demonstrating the tristate ion shutter in standalone ion mobility measurements, the
46 present study demonstrates the practical benefits of the tristate ion shutter in
47 multiplexing techniques (FT-IMMS) on a mixture of ion populations and a peptide with
48 multiple charged states. Moreover, higher gating frequencies of 5 - 10,005 Hz, 5 -
49 15,005 Hz and 5 - 20,005 Hz were implemented for the TXA salt mixture with higher ion
50
51
52
53
54
55
56
57
58
59
60

1
2
3 counts detected at a gating frequency of 5 - 10,005 Hz in the FT-IMMS experiments.
4
5 Similar results were also observed in the FT-IMMS experiments for bradykinin at the
6
7 same frequency sweep. In addition to the analytical benefits afforded by this shutter
8
9 configuration and the 3S-IS mode, our experiments detail an approach to assessing the
10
11 degree of peak overlap from adjacent ion gating events that aid experimentalists in
12
13 determining the optimum multiplexing parameters for ion mobility experiments. Given
14
15 the ease of implementation of the tri-grid shutter (i.e. does not require resource
16
17 intensive wire grids and manual gate construction) and the straight-forward operation of
18
19 the grid structure in a tri-state mode, the present effort provides a clear path for broad
20
21 implementation of this experimental approach for drift-tube IMS systems.

22 CONFLICTS OF INTEREST

23
24 There are no conflicts of interest to declare
25
26

27 ACKNOWLEDGEMENTS

28
29 Support for P.K-B. was provided by Army Research Office (Award# W911NF1510619).
30
31 The authors would also like to acknowledge NSF support (CHE-1506672).
32
33
34
35
36
37
38
39
40
41
42
43
44
45
46
47
48
49
50
51
52
53
54
55
56
57
58
59
60

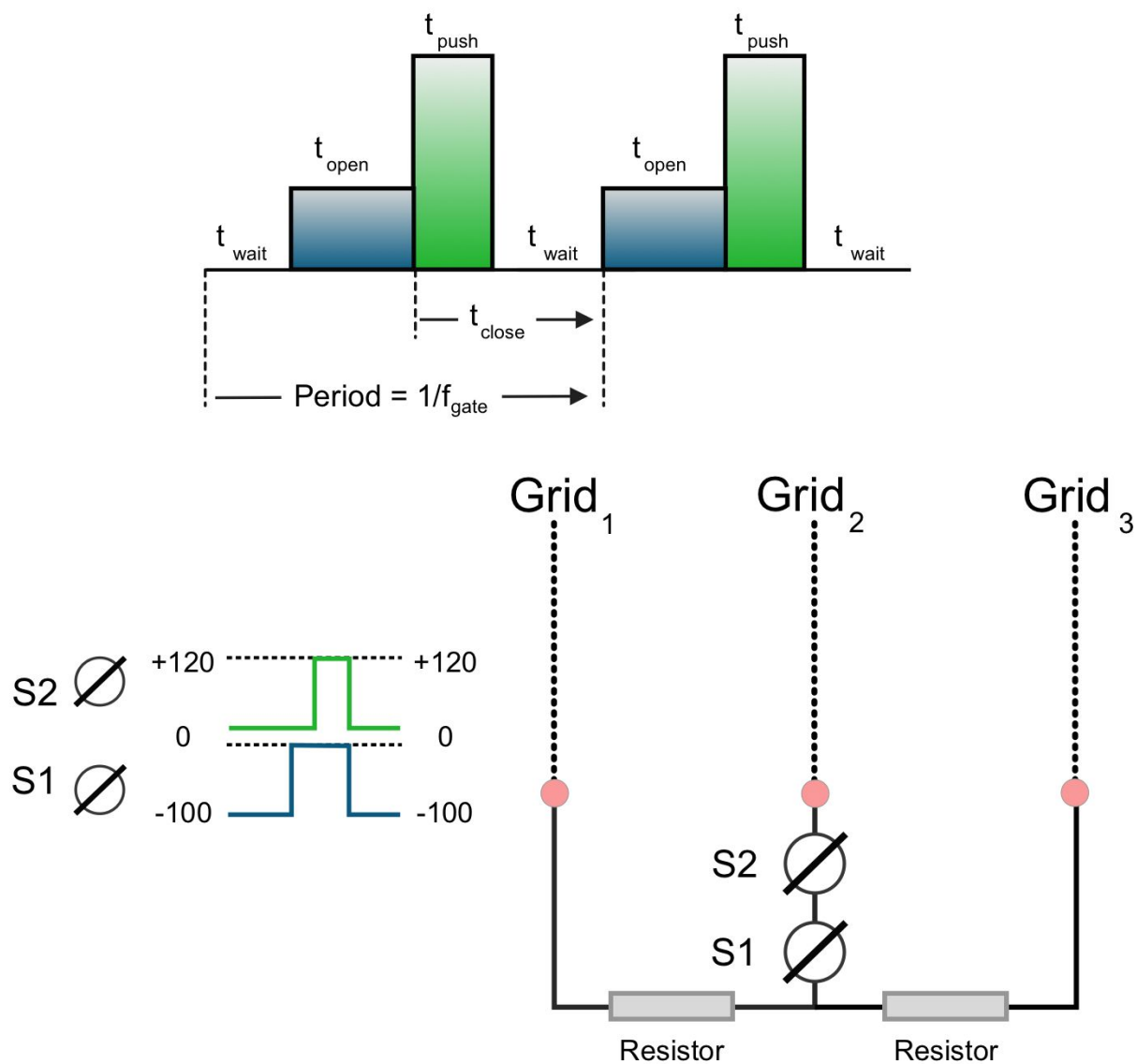


Figure 1. A schematic diagram of the tri-state ion shutter with its corresponding pulsing sequence employed in this study. Description of this schematic diagram can be found in the experimental section.

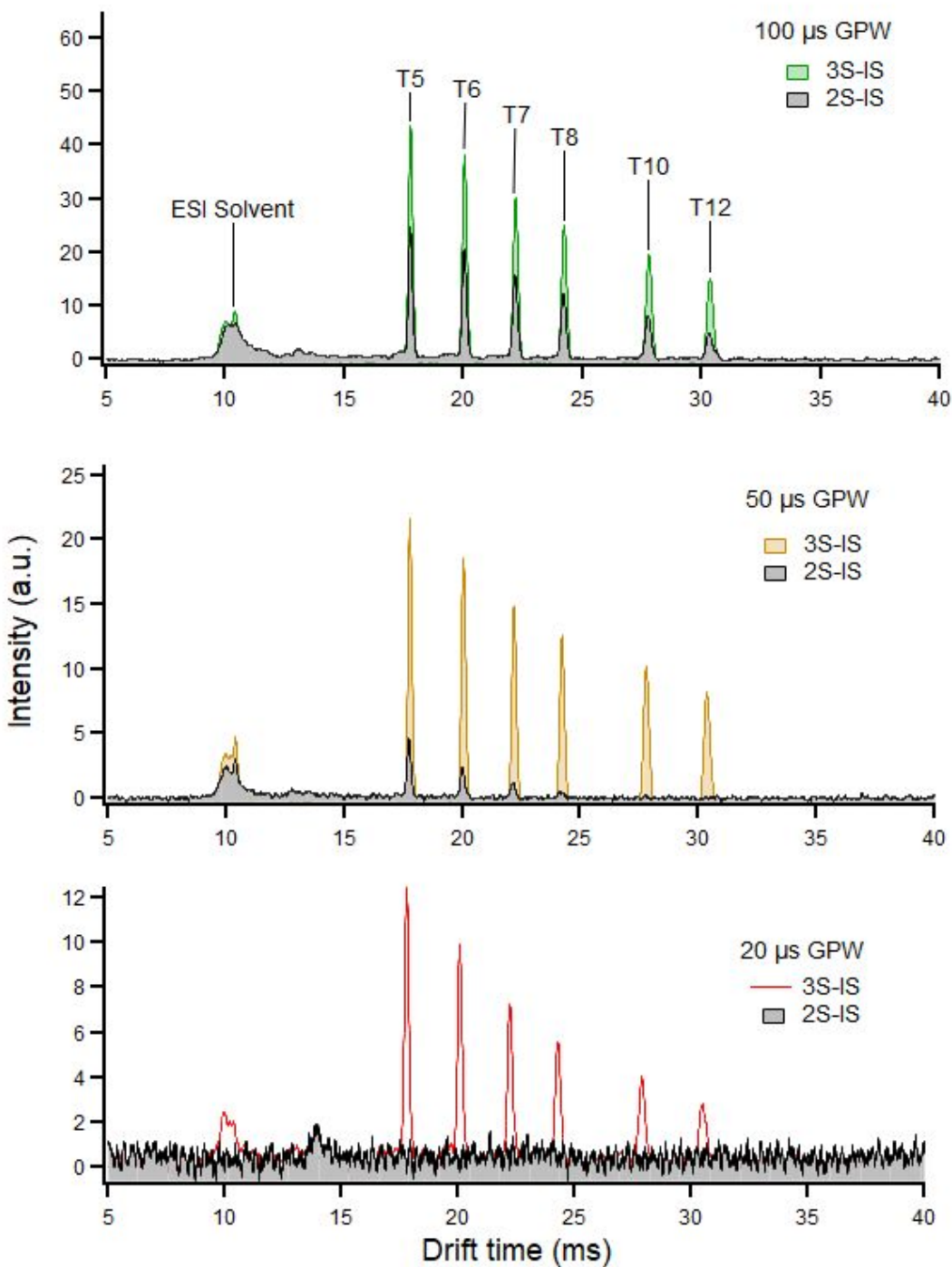


FIGURE 2. Standalone Faraday plate ion mobility spectra for a series of tetraalkylammonium salts (T5-T8, T10, T12) representing a wide range of reduced mobility values. The data were acquired using different gate pulse widths for the respective shutter operating conditions.

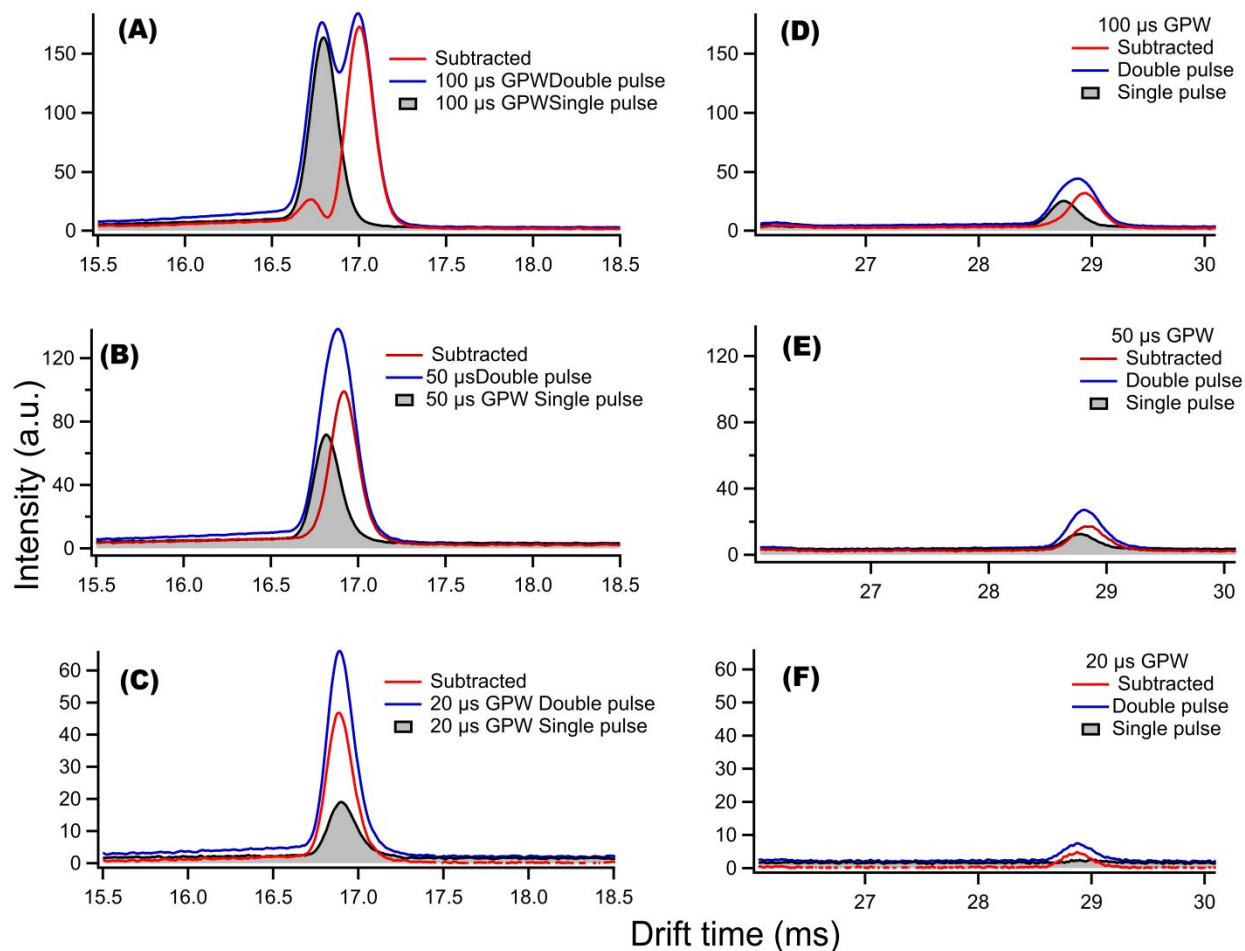


FIGURE 3. Stand alone ion mobility spectra with a zoomed-in effect for target analyte ion T5 at (A) 100 μ s, (B) 50 μ s (C) 20 μ s GPW and T12 ion at (D) 100 μ s, (E) 50 μ s (F) 20 μ s GPW for a single pulse sequence (black trace) and a double pulse sequence (blue trace) using the tristate ion shutter. The subtracted spectra (red trace) was obtained by subtracting the single pulse spectra from the double pulse spectra. The purpose of Figure 3 is to demonstrate the various parameterization steps that were investigated in order to effectively use the 3S-IS for multiplexing experiments.

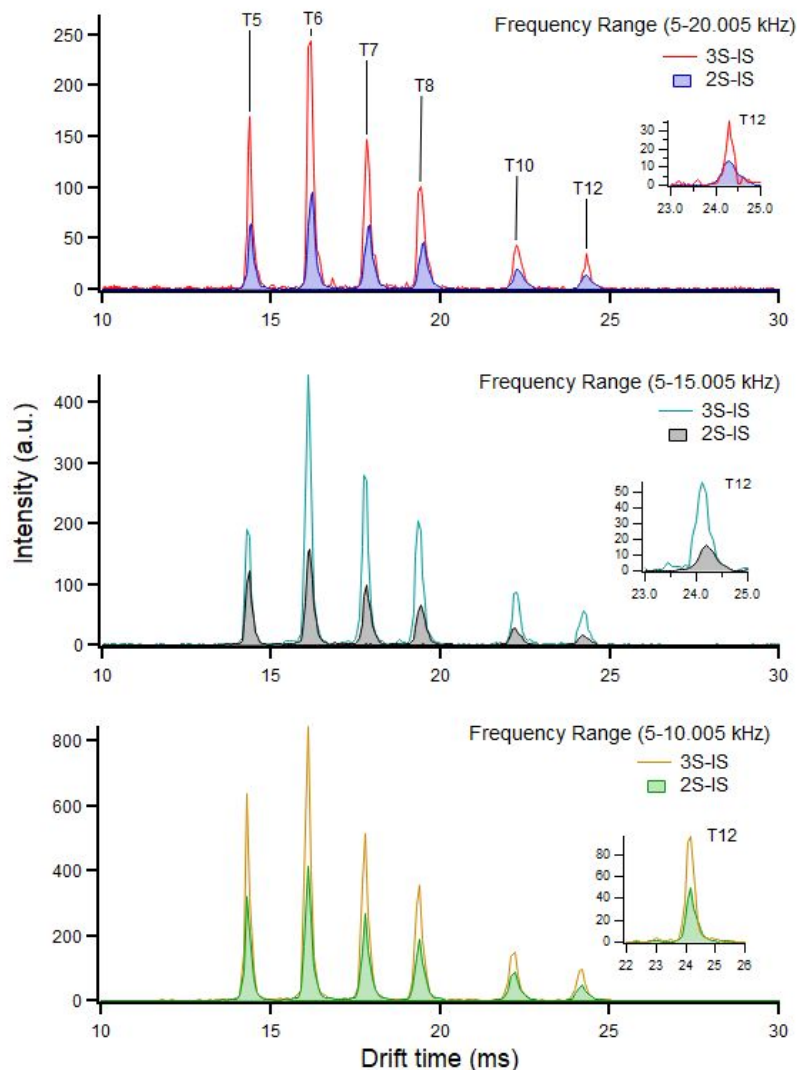


FIGURE 4. Mass selected mobility spectra from FT-IMMS experiment for 3 set of frequency sweeps using both the tristate ion shutter and the old ion shutter. The target analyte ions demonstrated in the spectra are tetraalkylammonium salts (T5-T8, T10, T12), also shown in Figure 2. The inserts are the zoomed in spectra for T12 ion with the following resolving power: 83, 79, 83 for a frequency range of 5-20,005 Hz, 5-15,005 Hz and 5-10,005 Hz respectively using the 3S-IS and 59, 63, 64 for a frequency range of 5-20,005 Hz, 5-15,005 Hz and 5-10,005 Hz respectively using the 2S-IS.

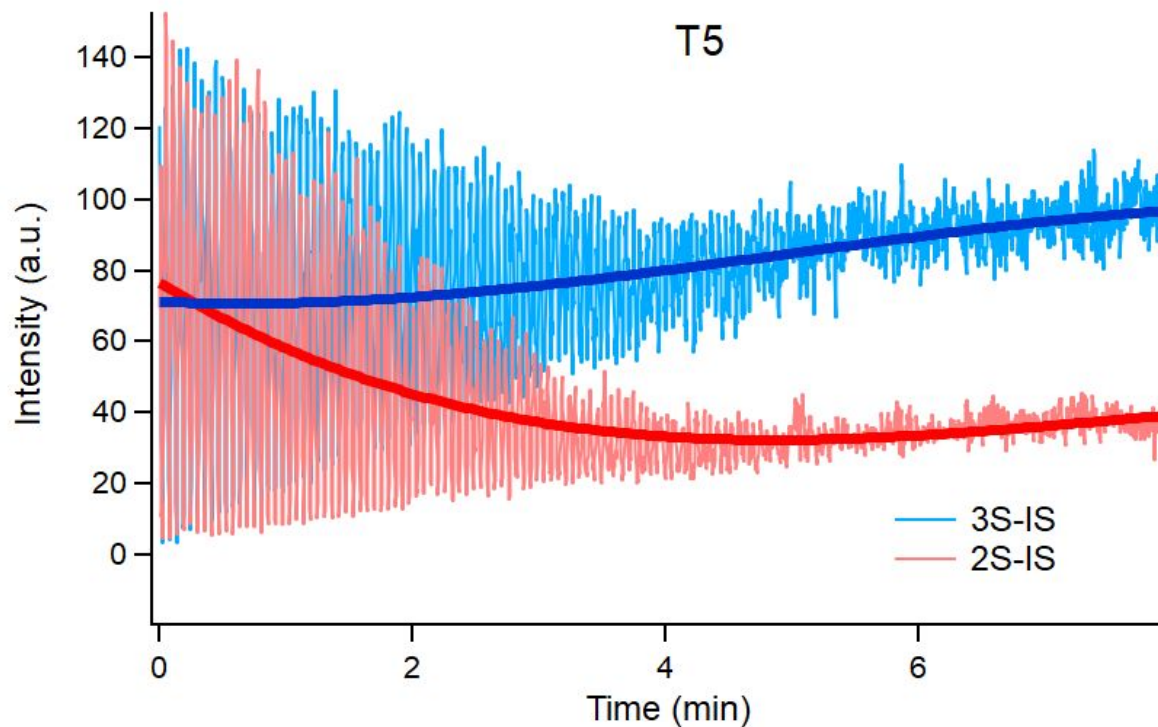


FIGURE 5. Supporting the ion current data presented in Table 1, two raw signal traces for the FT-IMMS experiment are shown with each corresponding to the different shutter principles under investigation. While the gains in resolving power following Fourier transformation are ~10% in favor of the 3S-IS, the increase in ion signal is substantial. This latter point is particularly relevant for ion mobility-mass spectrometry instruments where increases in ion current can aid deisotoping and tandem MS efforts.

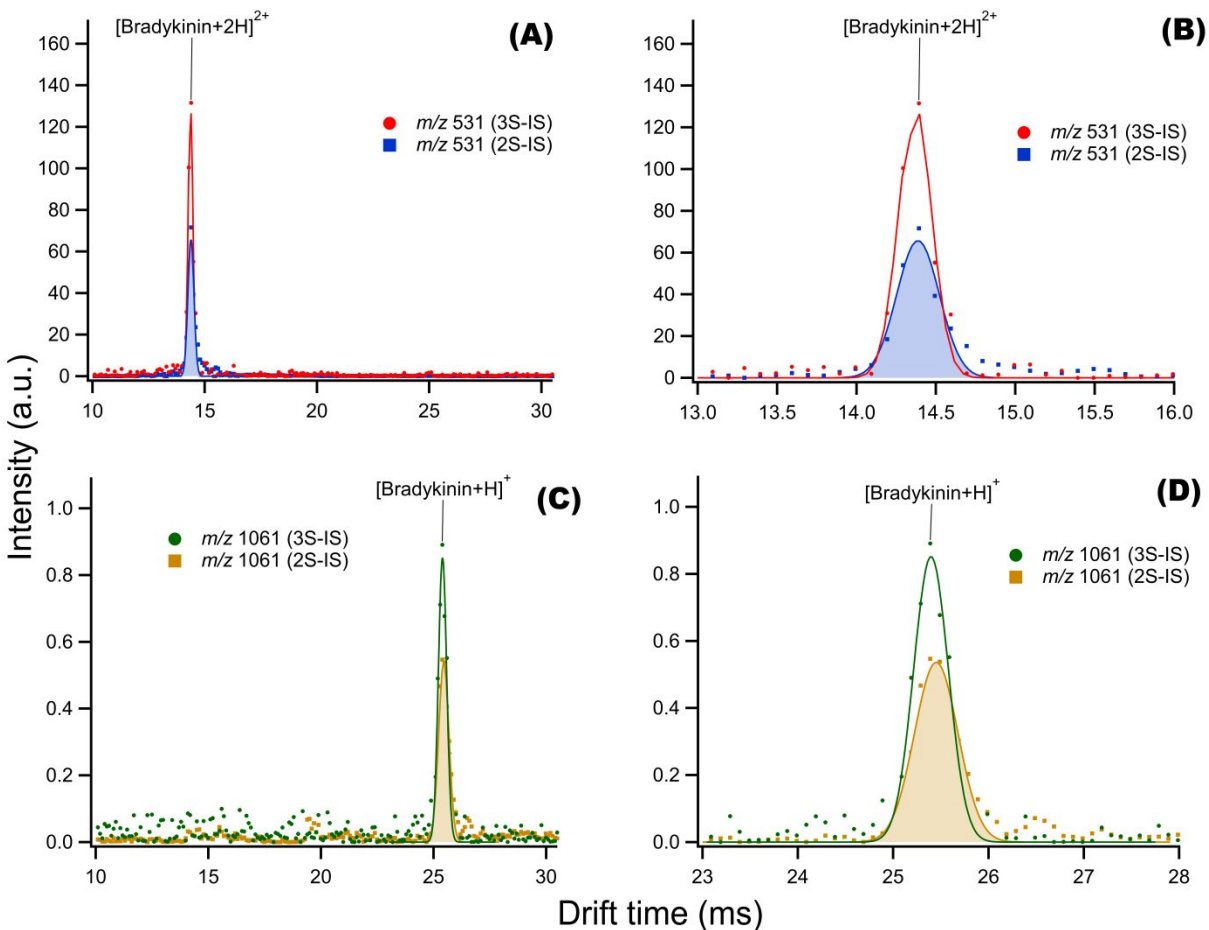


FIGURE 6. Mass selected mobility spectra obtained through the FT-IMMS experiment from 5-10005 Hz for 8 minutes using both the tri-state ion shutter and the two-state ion shutter. The markers represent peak distribution for the target analyte ions while the line traces are gaussian fits to the target analyte ion peaks. **(A)**, **(C)** are the mobility spectrum of $[\text{bradykinin}+2\text{H}]^{2+}$, $[\text{bradykinin}+\text{H}]^{+}$ respectively and **(B)**, **(D)** are zoomed in mobility spectrum of $[\text{bradykinin}+2\text{H}]^{2+}$, $[\text{bradykinin}+\text{H}]^{+}$ respectively.

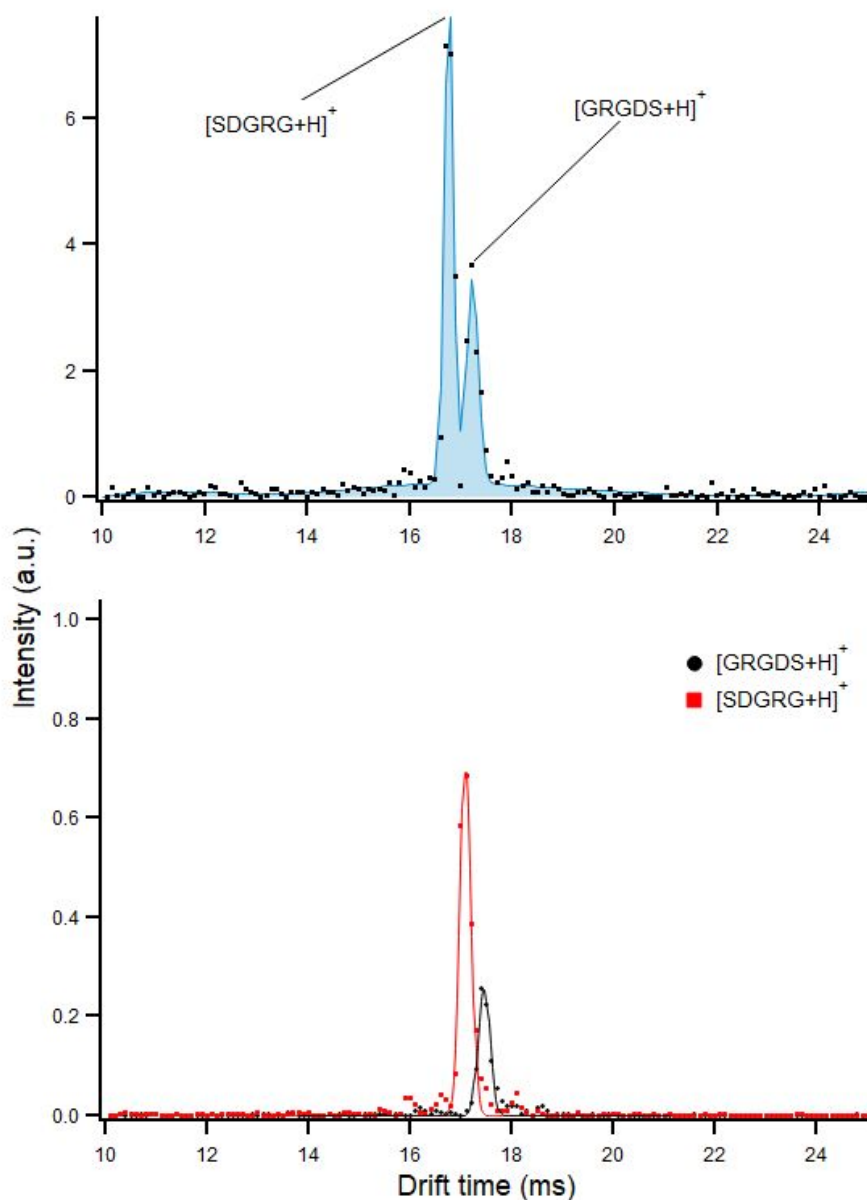


FIGURE 7. Mass selected mobility spectra obtained through the FT-IMMS experiment with a frequency sweep from 5-10005 Hz for 8 minutes using the tri-state ion shutter. The target analyte demonstrated in this figure is reversed sequence pentapeptide ([Ser-Asp-Gly-Arg-Gly], [Gly-Arg-Gly-Asp-Ser]). The top spectrum represents the mixture and the bottom spectrum represents the individual analytes. The markers represent peak distribution for the target analyte ions while the line traces are gaussian fits to the target analyte ion peaks.

TABLE 1. Summary of m/z , ion counts and resolving power for the target analyte ions using the tri-state ion shutter and two-state ion shutter.

Analyte	m/z	Ion counts		Resolving Power	
		3S-IS	2S-IS	3S-IS	2S-IS
T5	298	$2.05 \times 10^4 \pm 2 \times 10^3$	$1.05 \times 10^4 \pm 6 \times 10^2$	85 \pm 1	71 \pm 0.3
T6	354	$2.13 \times 10^4 \pm 3 \times 10^3$	$1.10 \times 10^4 \pm 4 \times 10^2$	81 \pm 1	71 \pm 0.4
T7	410	$1.75 \times 10^4 \pm 2 \times 10^3$	$9.06 \times 10^3 \pm 5 \times 10^2$	77 \pm 0.4	69 \pm 0.2
T8	466	$1.67 \times 10^4 \pm 7 \times 10^2$	$6.87 \times 10^3 \pm 6 \times 10^1$	76 \pm 2	67 \pm 1
T10	578	$9.54 \times 10^3 \pm 5 \times 10^2$	$5.30 \times 10^3 \pm 2 \times 10^1$	75 \pm 0.4	66 \pm 0.4
T12	690	$6.69 \times 10^3 \pm 6 \times 10^2$	$4.47 \times 10^3 \pm 6 \times 10^1$	83 \pm 1	66 \pm 0.3
Bradykinin (+1 charge)	1061	$1.35 \times 10^3 \pm 2 \times 10^2$	$8.69 \times 10^2 \pm 9 \times 10^1$	72 \pm 0.3	62 \pm 1

state)					
Bradykinin (+2 charge state)	531	$6.25 \times 10^4 \pm 5 \times 10^2$	$4.89 \times 10^3 \pm 3 \times 10^2$	70 ± 0.4	65 ± 0.3

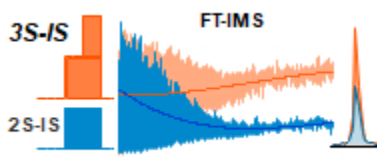
Ion counts recorded in Table 1 were reported from the raw mass spectrum of the FT-IMMS experiments from 5 to 10005 Hz (100 μ s effective GPW) for 8 minutes and not the transformed arrival time distribution of the FT-IMMS.

REFERENCES

- 1 C. Laphorn, F. Pullen and B. Z. Chowdhry, *Mass Spectrom. Rev.*, 2013, **32**, 43–71.
- 2 P. Dwivedi, G. Puzon, M. Tam, D. Langlais, S. Jackson, K. Kaplan, W. F. Siems, A. J. Schultz, L. Xun, A. Woods and H. H. Hill Jr, *J. Mass Spectrom.*, 2010, **45**, 1383–1393.
- 3 G. Reid Asbury, J. Klasmeier and H. H. Hill Jr, *Talanta*, 2000, **50**, 1291–1298.
- 4 F. W. Karasek, H. H. Hill Jr and S. H. Kim, *J. Chromatogr.*, 1976, **117**, 327–336.
- 5 W. E. Steiner, S. J. Klopsch, W. A. English, B. H. Clowers and H. H. Hill, *Anal. Chem.*, 2005, **77**, 4792–4799.
- 6 M. Mäkinen, M. Nousiainen and M. Sillanpää, *Mass Spectrom. Rev.*, 2011, **30**, 940–973.
- 7 S. R. Harvey, C. E. Macphee and P. E. Barran, *Methods*, 2011, **54**, 454–461.
- 8 C. Uetrecht, R. J. Rose, E. van Duijn, K. Lorenzen and A. J. R. Heck, *ChemInform*, 2010, **41**, no–no.
- 9 E. Jurneczko and P. E. Barran, *Analyst*, 2011, **136**, 20–28.
- 10 S. I. Merenbloom, S. L. Koeniger, S. J. Valentine, M. D. Plasencia and D. E. Clemmer, *Anal. Chem.*, 2006, **78**, 2802–2809.
- 11 J. P. Williams, H. I. A. Phillips, I. Campuzano and P. J. Sadler, *J. Am. Soc. Mass Spectrom.*, 2010, **21**, 1097–1106.
- 12 A. T. Kirk, C.-R. Raddatz and S. Zimmermann, *Anal. Chem.*, 2017, **89**, 1509–1515.
- 13 B. H. Clowers and H. H. Hill, *Analytical Chemistry*, 2005, **77**, 5877–5885.
- 14 F. W. Karasek, W. D. Kilpatrick and M. J. Cohen, *Anal. Chem.*, 1971, **43**, 1441–1447.
- 15 T. Reinecke, C. N. Naylor and B. H. Clowers, *Trends Analyt. Chem.*, 2019, **116**, 340–345.
- 16 K. A. Morrison, W. F. Siems and B. H. Clowers, *Anal. Chem.*, 2016, **88**, 3121–3129.
- 17 M. L. Poltash, J. W. McCabe, M. Shirzadeh, A. Laganowsky, B. H. Clowers and D. H. Russell, *Anal. Chem.*, 2018, **90**, 10472–10478.
- 18 X. Tang, J. E. Bruce and H. H. Hill Jr, *Rapid Commun. Mass Spectrom.*, 2007, **21**, 1115–1122.
- 19 F. J. Knorr, R. L. Eatherton, W. F. Siems and H. H. Hill Jr, *Anal. Chem.*, 1985, **57**, 402–406.
- 20 B. H. Clowers, W. F. Siems, Z. Yu and A. L. Davis, *Analyst*, 2015, **140**, 6862–6870.
- 21 J. Puton, A. Knap and B. Siodłowski, *Sens. Actuators B Chem.*, 2008, **135**, 116–121.
- 22 N. E. Bradbury and R. A. Nielsen, *Phys. Rev.*, 1936, **49**, 388–393.
- 23 Y. M. Ibrahim, S. V. B. Garimella, A. V. Tolmachev, E. S. Baker and R. D. Smith, *Anal. Chem.*, 2014, **86**, 5295–5299.
- 24 J. Langejuergen, M. Allers, J. Oermann, A. Kirk and S. Zimmermann, *Anal. Chem.*, 2014, **86**, 7023–7032.
- 25 W. C. Blanchard, E. G. Nazarov, J. Carr and G. A. Eiceman, *Int. J. Ion Mobility Spectrom.*, 2002, **5**, 15–18.
- 26 T. Reinecke, A. L. Davis and B. H. Clowers, *J. Am. Soc. Mass Spectrom.*, 2019, **30**, 977–986.

- 1
2
3 27 A. T. Kirk, D. Grube, T. Kobelt, C. Wendt and S. Zimmermann, *Anal. Chem.*, 2018,
4 **90**, 5603–5611.
5 28 C. Thoben, C. Raddatz, A. T. Kirk and S. Zimmermann, in *Sensors and Measuring*
6 *Systems; 19th ITG/GMA-Symposium*, 2018, pp. 1–4.
7 29 T. Reinecke and B. H. Clowers, *HardwareX*, 2018, **4**, e00030.
8 30 T. Reinecke, A. T. Kirk, A. Ahrens, C.-R. Raddatz, C. Thoben and S. Zimmermann,
9 *Talanta*, 2016, **150**, 1–6.
10 31 L. Garcia, C. Saba, G. Manocchio, G. A. Anderson, E. Davis and B. H. Clowers, *Int.*
11 *J. Ion Mobil. Spectrom.*, 2017, **20**, 87–93.
12 32 M. F. Bush, Z. Hall, K. Giles, J. Hoyes, C. V. Robinson and B. T. Ruotolo, *Anal.*
13 *Chem.*, 2010, **82**, 9557–9565.
14 33 B. Harper, E. K. Neumann, S. M. Stow, J. C. May, J. A. McLean and T. Solouki,
15 *Anal. Chim. Acta*, 2016, **939**, 64–72.
16
17
18
19
20
21
22
23
24
25
26
27
28
29
30
31
32
33
34
35
36
37
38
39
40
41
42
43
44
45
46
47
48
49
50
51
52
53
54
55
56
57
58
59
60

1
2
3
4
5
6
7
8
9
10
11
12
13
14
15
16
17
18
19
20
21
22
23
24
25
26
27
28
29
30
31
32
33
34
35
36
37
38
39
40
41
42
43
44
45
46
47
48
49
50
51
52
53
54
55
56
57
58
59
60



76x39mm (72 x 72 DPI)